

# Can sub-GeV dark matter coherently scatter on the electrons in the Atom?

Ji-Heng Guo, Yu-Xuan Sun, Wenyu Wang, Ke-Yun Wu\*  
*Faculty of Science, Beijing University of Technology, Beijing, China*

A novel detection of sub-GeV dark matter is proposed in the paper. The electron cloud are boosted by the dark matter and throw away an electron when it is dragged back by the heavy nucleus, namely the coherent scattering of the electron cloud of the atom. The survey in the X-ray diffraction shows that the atomic form factor are much complicate than the naive consideration. The results of the relativistic Hartree-Fock method gives non-trivial shapes of the atom. The detailed calculation of recoil of the electron cloud. The kinetics, the fiducial cross section and the corresponding calculation of detection rate are given analytically. The numerical results show that the limits of the RHF form factor are much stringent than the recoil of a single electron, almost 4 orders stronger. The limits on the RHF form factor are more stringent than the Migdal effect below about several hundred MeV. The physical picture and the corresponding results are promising and need further explorations.

## I. INTRODUCTION

Observations in cosmology and astrophysics clearly support the presence of dark matter (DM) [1]. Its features, such as mass and interactions are however still unknown. One of the most promising experimental avenues is to search for the small energy depositions from the dark matter elastically scattering in sensitive detectors on Earth. An attractive dark matter candidate is Weakly Interacting Massive Particles (WIMPs), which have been explored in various direct detection, indirect detection and collider experiments. The null results have produced very stringent limits on the WIMP-nucleus scattering cross section heavier than 1 GeV. Thus the hunt for sub-GeV dark matter is a hot topic at the cutting edge of physics research. However, as the sensitivity lost for the light dark matter detection, the traditional strategies for detecting WIMP-type dark matter are no longer feasible. Physicists are striving to create techniques for detecting light dark matter.

Among all the new ways for searching the sub-GeV dark matter, the ionization signal on the detectors could be the most promising one. In the dual-phase Xenon Time Projection Chamber, the xenon atoms in the Liquid Xenon phase can be ionized due to a collision. Then the ionized electrons drift into the Gaseous Xenon layer at the top of the detector in presence of an external electric field, which produces a proportional scintillation light, namely the S2 signal. In the theoretical studies, such ionization signals can come from the DM-electron scattering [2–10] or the DM-nucleus scattering through the Migdal effect that originates from non-instantaneous movement of electron cloud during a nuclear recoil event [11–27].

In addition to those DM-electron scattering and the Migdal effect on the ionization detection, there is another way which seems to promising for the search of the light dark matter. As talked in the textbooks that the electrons which are bounded by the nucleus in an atom to form the electron cloud. If the dark matter can collide with the single electron in the atom, it can also collide the whole cloud of the atom too. In fact, this is just the coherent scattering in the dark matter detection. For example, there can be  $Z^2$  (charge number) or  $A^2$  (atom number) enhancements in the spin-independent detection of the DM-nucleus scattering. As for the detection of the ionization, the question is that does similar coherent enhancement exist in the recoils of the electron. This is not a stupid question since it can be seen in the X-ray diffraction (XRD) on the atom, there do have the coherent scattering of electron cloud from which the atom scattering form factor can be derived. As for the sub-GeV dark matter, the DeBroglie wavelength of the dark matter can be sufficiently small enough to inject into the target atom, the same as the diffraction of the incident X-ray too. The collision can boost the electron cloud to a sizable velocity, After that it can also be dragged back by the static heavy nucleus and throw away an electron to give similar ionization S2 signal. Such mechanism seems reasonable, or at least should be checked that whether this effect can exist or can be significant of the detection.

In this paper, we will check this novel detection of scattering of the electron cloud to see whether a coherent enhancement exists in the recoils of the electron. As the process is similar to the diffraction of X-ray scattering on the atom, we will show our understanding in the coherent scattering from the point of the X-ray diffraction at first. Then we will show how to calculate the coherent scattering between dark matter and the electron cloud. After that, the constraints from the current dark matter detection are calculated numerically for the comparison with the results

---

\*Electronic address: [294483554@emails.bjut.edu.cn](mailto:294483554@emails.bjut.edu.cn), [YuXuanSun@emails.bjut.edu.cn](mailto:YuXuanSun@emails.bjut.edu.cn), [wyyang@bjut.edu.cn](mailto:wyyang@bjut.edu.cn), [keyunwu@emails.bjut.edu.cn](mailto:keyunwu@emails.bjut.edu.cn)

of the DM-electron scattering and the Migdal effect. The paper is organized in the following: the coherent scattering of the electron in an atom are discussed in the sec. II; the calculation methodology are given in the sec. III; the numerical results and the comparison with the other strategies are shown in the sec. IV and our conclusion is given in the sec. V.

## II. COHERENT SCATTERING OF THE ELECTRON IN AN ATOM

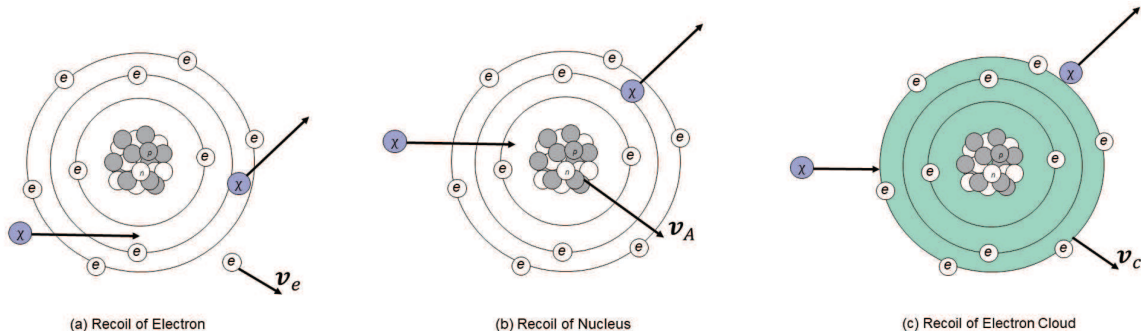


FIG. 1: The three processes which can induce ionization which are the collision between dark matter and single electron, the Migdal effect and the collision between dark matter and the electron cloud of an atom, respectively.

Fig. 1 shows the scattering processes of the electrons when the dark matter collide on the atom in which Fig. 1 (a) shows sketch map of that the dark matter scattering on the single electron and Fig. 1 (b) shows the sketch map of the Migdal effect. Detailed calculation of the first two processes and the comparison between them can be found in Ref. [19]. Here we just list essential points of these two processes:

1. In the recoil of the electron, the dark matter transfers momentum  $q$  directly to the single electron bounded in the atom, giving the ionization electron with recoil energy  $E_e$  and momentum  $k_e$ . The impulse approximation[28] can be adopted in the theoretical calculation of the rate.
2. For the Migdal effect, the dark matter transfer momentum  $q$  to the nucleus. The momentum transfer happens much faster than the light-crossing time of the electron cloud, thus the nucleus get a sudden "movement" with velocity  $v_A$  which can drag the electron cloud to same velocity and throw away an electron with energy  $E_e$  and momentum  $k_e$ . The inner product of the containing phase between the eigenstate wave function at rest and the Galilean transformation of the energy eigenstates of the moving atom gives the amplitude of the throwing rate of electron.
3. The numerical results show that the Migdal effect is always subdominant to the electron scattering when the mediator is light. But it can dominate the ionization for heavy mediator and mass of the dark matter in hundreds of MeV range.

In addition to these two processes, we focus on another novel collision between the dark matter and the electron cloud which is formed by the bounded electrons in an atom. The corresponding sketch map of the process is shown in the Fig. 1 (c). The electron cloud is taken as a "all" composed of the distributed electric charge of which the amount is the charge number of the corresponding target element. As the mass of the dark matter is at the MeV order, one can simply figure out the DeBroglie wavelength of the dark matter is much smaller than the radius of the target atom which is about several Bohr radii. Thus the collision between dark matter and the electron cloud can be considered as a collision between a "point" and a "puffy ball". [29, 30] The corresponding scattering rate is always conveniently calculated in the momentum space, and the Fourier transformation of the charge distribution  $\rho(r)$  gives the form factor  $F(q)$  to account for the coherence of the charge distribution. The whole picture is similar to the diffraction of X-ray scattering on the crystal, thus before going to further exploration the detection of the dark matter, we discuss some essentials of X-ray diffraction.

The X-ray diffraction is a powerful tool widely used in research and industry. While XRD is usually well known for qualitative and quantitative analyses of crystalline phases in materials, far more information can be obtained from a careful analysis of the diffraction patterns or by using specific XRD settings: i.e. characterization of solid solutions, crystallite size and shape, crystal orientation, et al. In XRD analyses, the diffraction of a wave of the characteristic

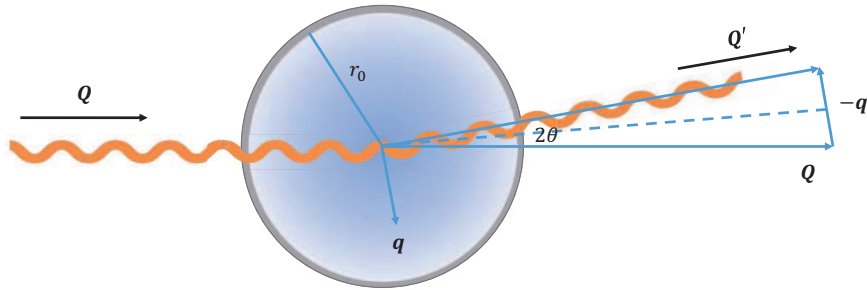


FIG. 2: The X-ray diffraction on the atom.

length  $\lambda$  is required to be of the same size as the interatomic separation of the crystal. However, XRD are in fact can also detect the inter-structure of a specific atom which is called the small-angle techniques of which the sketch map is shown in the Fig. 2. Such small-angle technique is a method of the investigation of the non-periodic systems. The physics principles of the scattering are the same for both wide-angle diffraction and the small-angle diffraction, in which the angle-dependent scattering amplitude is related to the electron-density distribution of the scatterer by a Fourier transformation. The main difference between wide- and small-angle diffraction in XRD is that we have a periodic arrangement of identical scattering centers (particles) in wide-angle diffraction, while the scattering center are limited in size, non-oriented, and non-periodic, but the number of the particles is high and the can be assumed to be identical of the small-angle diffraction. Thus the small-angle diffraction can give a detailed investigation a single target. There are both coherent and incoherent scattering in the X-ray diffraction, and for the scattering on a single electron they are called Rayleigh scattering and Compton scattering, respectively. As shown in the Fig. 2, the momentum transfer  $q$  to the electron can be easily derived from the small-angle deviation from the incident X-ray, thus the parameter  $\sin \theta/\lambda$  are always adopted for the description of the form factor is the momentum space with the relation

$$\frac{\sin \theta}{\lambda} = \frac{q}{4\pi}. \quad (1)$$

The summation of all the electrons gives the atomic scattering form factor

$$F(q) = \sum_j^Z f_j = \sum_j^Z \int \rho(\mathbf{r}_j) \exp(\mathbf{q} \cdot \mathbf{r}_j) d\mathbf{r}_j. \quad (2)$$

For the scattering by the atomic electrons, the phase of coherent scattering is by convention related to that of the a free electron at the nucleus. There is a phase shift of  $\pi$  for scattering from a free electron. And the coherent scattering in the XRD is

$$I_{\text{coh}} = I_e (F(q))^2. \quad (3)$$

In above equation,  $I_e$  is the intensity of the scattering per unit solid angle which are calculated from the Thomson formula

$$I_e = I_0 r_e^2 \left[ \frac{1 + 2 \cos^2 \theta}{2} \right], \quad (4)$$

in which  $I_0$  is the intensity of the unpolarized incident beam and  $r_e$  is the classical radius of the electron ( $2.818 \times 10^{-15} \text{m}$ ). Note that  $I_e$  and  $I_0$  have different dimensions. Another issue should be mentioned is that the momentum of the incident X-ray  $Q$  is much greater than the momentum transfer  $q$ . This means that the wavelength of incident X-ray are much smaller than the inverse momentum transfer  $\lambda_X \ll 1/q$ . Thus above calculations are reliable in case of the wavelength of the X-ray larger than the classical radius of the electron, no matter how large the atom is. This is the key point of the understanding of the XRD which can be simply applied to the scattering of the dark matter. The details are talked in the next section.

It is usually considered as a common sense that the atomic form factor  $F(q)$  could be described by a function equals the charge number  $Z$  at zero momentum transfer and roughly decrease with the inverse of the atom radius quickly. However, things are contrary to the usual expectation. For the Hydrogen atom,  $F(q)$  can be got analytically by solving the Schrödinger equation and it is effectively zero for  $\sin\theta/\lambda > 1.5\text{\AA}^{-1}$ . Those for heavier atoms are for relativistic wavefunctions which can be calculated by Relativistic Hartree-Fock (RHF) method of which the details can be found in Refs. [31, 32] and all the results are summarized and listed in Ref. [33]. Usually, the form factor can be effectively described by Gaussian fits in the range  $0\text{\AA}^{-1} < (\sin\theta)/\lambda < 2.0\text{\AA}^{-1}$

$$f(\sin\theta/\lambda) = \sum_{i=1}^4 a_i \exp(-b_i \sin^2\theta/\lambda^2) + c.$$

Take Xenon as an example, the fit parameters in above equation are  $a_1 = 20.2933$ ,  $b_1 = 3.9282$ ;  $a_2 = 19.0298$ ,  $b_2 = 0.344$ ;  $a_3 = 8.9767$ ,  $b_3 = 26.4659$ ;  $a_4 = 1.99$ ,  $b_4 = 64.2658$ ;  $c = 3.7118$ . But as the angle increases to  $2.0\text{\AA}^{-1} < (\sin\theta)/\lambda < 6.0\text{\AA}^{-1}$ , Ref. [34] have shown that the fitting formula above is highly inaccurate, as the scattering angle increasing, and they produced a 'logarithmic polynomial' curve-fitting routine based on the equation

$$\ln\{f[(\sin\theta)/\lambda]\} = \sum_{i=0}^3 c_i s^i, \quad (5)$$

for these high angles. Also take Xenon as an example, the  $c_i$  values are  $c_0 = 4.24610$ ,  $c_1 = -1.56330$ ,  $c_2 = 3.04200$ ,  $c_3 = -2.34290$  give a close fit to the atomic scattering factor curves over the range and the correlation coefficient is 0.999.

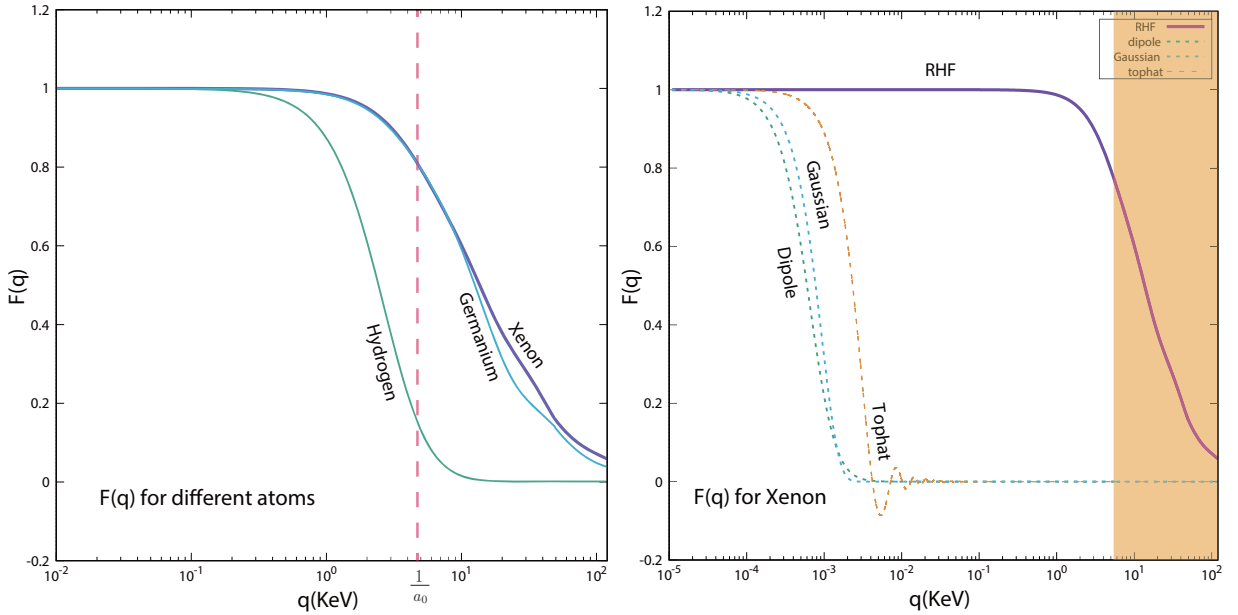


FIG. 3: Left: the atomic form factor of Hydrogen, Germanium and Xenon in which the Hydrogen's is calculated analytically from Schrödinger Equation, and the other two are calculated by Relativistic Hartree-Fock method. The corresponding momentum of inverse Bohr radius  $1/a_0$  is shown in dash line. Right: Xenon  $F(q)$  got form tophat, Gaussian, dipole and the RHF method. The orange shade is the interval of momentum transfer  $q$  in the detection of light dark matter. All the form factors are normalized to 1 at zero momentum transfer  $q = 0$  for the comparison.

In order to show the difference, we show the form factor  $F(q)$  for Hydrogen, Germanium and Xenon in the left panel of the Fig. 3 in which the Hydrogen form factor is calculated analytically from Schrödinger Equation, and the other two are calculated by RHF. The corresponding momentum of inverse Bohr radius  $1/a_0$  is shown in the panel. Note that all the form factors are normalized to 1 at zero momentum transfer  $q = 0$  for the comparison. The form factor of Hydrogen is a dipole form, and it decrease will the momentum transfer  $q$  very quickly. As for the Germanium and Xenon of which the radii are about four times Bohr radius, contrary to the common sense, the

$F(q)$  do not decrease at the border of inverse radius. They can maintain a sufficiently large value to the much larger  $q \gg 1/a_0$ . Then how about the shape of the atom? Usually physicist use following three kinds of the shapes to describe an atom with specific size  $r_0$ [29, 30]

Shape	$\rho(r)$	$r_{\text{Atom}}$	$F(q)$
tophat	$\frac{3}{4\pi r_0^3} \theta(r_0 - r)$	$\sqrt{3/5} r_0$	$\frac{3(\sin(r_0 q) - r_0 q \cos(r_0 q))}{r_0^3 q^3}$
dipole	$\frac{e^{-r/r_0}}{8\pi r_0^3}$	$2\sqrt{3} r_0$	$\frac{1}{(1+r_0^2 q^2)^2}$
Gaussian	$\frac{1}{8r_0^3 \pi^{3/2}} e^{-r^2/(4r_0^2)}$	$\sqrt{6} r_0$	$e^{-r_0^2 q^2}$

In above table, the middle column is the root-mean-square of the atom. The corresponding form factor  $F(q)$  of these three shapes together with the RHF result for Xenon are shown in the right panel of the Fig. 3 in which  $r_0 = 4a_0$ . The orange shade in the panel shows the interval of momentum transfer  $q$  for the detection of light dark matter which will be talked in the next section. We can see that the factors of the ordinary shapes decrease very quickly with  $q$ , but the RHF form factor implies a non-trivial shape of the atom.

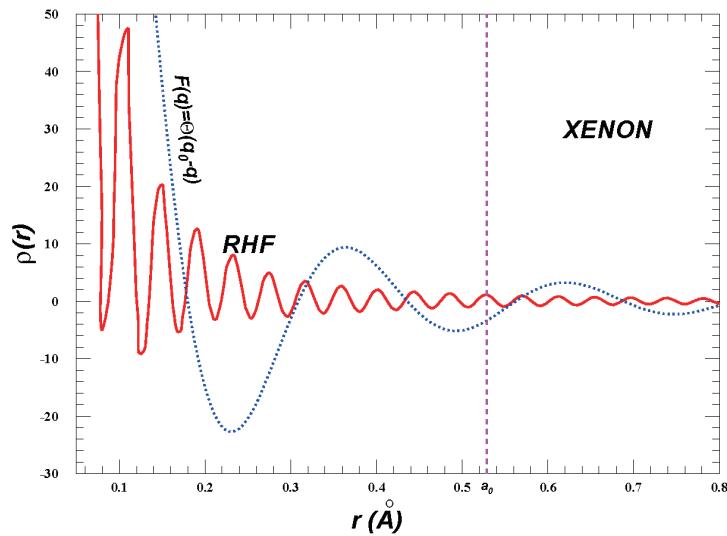


FIG. 4: Charge distribution of  $\rho(r)$  of Xenon, calculated by the Fourier transformation of RHF  $f(q)$  (red solid line) and a tophat model (blue dot line) in momentum space that  $F(q) = \theta(q_0 - q)$  with  $q_0 = 25\text{KeV}$ . The dash line shows the position of Bohr radius.

A slowly decreasing Form factor at a typical momentum  $q_0$  does not imply that radius of the atom at the order of  $1/q_0$ . Take a tophat distribution in the momentum space as an example

$$F(q) = \theta(q_0 - q), \quad (6)$$

The shape of the charge distribution is similar

$$\rho(r) = \frac{\sin(q_0 r) - q_0 r \cos(q_0 r)}{2\pi^2 r^3}. \quad (7)$$

The corresponding  $\rho(r)$  can be calculated by the Fourier transformation of  $F(q)$ , shown in the Fig. 4, in which we chose  $q_0 = 25\text{KeV}$  for the demonstration. The  $\rho(r)$  of Xenon atom numerically calculated from RHF form factor  $F(q)$  is shown in the red solid line of the figure. One can easily check that the root-mean-square radii in both cases are oscillating divergent functions. Though it decreases quickly along with the increase of the radius, the charge density can maintain the oscillating behavior to the large radius. Thus the non-trivial shape can make the form factor much different from the ordinary consideration.

From the Fig. 3 we can see that RHF Xenon  $F(q) \sim 0.2$  at  $q = 50\text{KeV}$ . The physics picture is that the momentum transfer  $q$  is much larger than  $1/r_0$ , then since it is a small angle scattering  $Q \gg q$ , the wavelength of X-ray is much smaller than the radius of the atom. This means that a much smaller X-ray photon which can inject into the interior of the atom can still transfer a much larger momentum to the whole atom and strongly interact with it. Whether such picture can happen in case of an incident dark matter? This will be discussed in the next section.

### III. RECOIL OF THE ELECTRON CLOUD AND ITS IONIZATION

Compare to the XRD, the key difference in the scattering between the dark matter and the atom may be the incident particle is massive and slowly moving. However, our focus is the sub-GeV dark matter with a velocity as several hundred kilometers per second  $\mathcal{O}(10^{-3}c)$ . Then the DeBroglie wave length for the dark matter lighter than 100 MeV can be much larger than the classical radius of the electron. If the interaction between the dark matter and electron are a compact, the time scale of the momentum transfer will also be much quicker than the light-crossing time of the electron cloud. The only problem is that the light-crossing time of the slowly moving dark matter is much longer than the X-ray, then non-trivial collision may happen. However, the whole picture is that whether the electron cloud can react as a compact ball in the collision process. The right panel of the Fig. 3 show that such compactness can only maintain at a much smaller momentum transfer regime  $q < 1/r_0$  for the ordinary tophat, dipole or Gaussian shape. But the RHF results show that the compactness could be reliable to a much higher  $q$ . If the compactness maintains, the longer collision time implies the collision can be considered as to have higher order collisions like the loop diagram, thus the amplitude must be at sub-leading order, as shown in the Fig. 5. In all, the collision between the dark matter and the electron electron cloud are analogous to the XRD. The collision between dark matter and the electron can transfer a much larger momentum to the whole electron cloud. The RHF form factor  $F(q)$  could be used for the estimation of the momentum transfer and the cross section. In the following, we will give a detailed study on this recoil of electron cloud (REC) to see whether such estimation is suitable for the exploration of the dark matter.

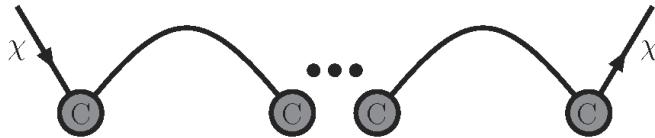


FIG. 5: Higher order collision between the dark matter and the electron cloud.

Following Ref. [19], the model consists a dark matter candidate  $\chi$ , which scatters off electrons through the exchange of a quite heavy dark photon  $A'$ . The Lagrangian is

$$\mathcal{L} = -\frac{1}{4}F'_{\mu\nu}F'^{\mu\nu} + \frac{m_{A'}^2}{2}A'_\mu A'^\mu + A'_\mu(g_D J_D^\mu + \epsilon e J_{EM}^\mu)$$

and the fiducial non-relativistic cross section for  $\chi$  scattering off a free-particle target  $T$  is defined at a reference 3-momentum transfer  $q_0 = \alpha m_e$  as

$$\bar{\sigma}_T = \frac{16\pi\epsilon^2\alpha\alpha_D\mu_{\chi T}^2}{(m_{A'}^2 + |q_0|^2)^2} \quad (8)$$

where  $\mu_{\chi T}$  is the reduced mass of the  $\chi - T$  system.

Next, we show the kinetics of the REC and compare it with the Migdal effect and recoil of a single electron. In all these processes, the incoming and outgoing states are the same: a dark matter particle plus a bound atom and a dark matter particle plus an ionized atom plus an unbound electron, respectively. The incoming dark matter is assumed to be a plane wave, which is both an energy eigenstate and a momentum eigenstate. The incoming atom (at rest in the lab frame) is an energy eigenstate and a momentum eigenstate too. The outgoing dark matter is also a plane wave, and the outgoing atom is in an excited state where the ionized electron belongs to the continuum spectrum of the atomic Hamiltonian. Consider the scattering process of a dark matter particle hitting electron clouds of  $Z$  electrons outside the entire nucleus, for the dark matter particle with mass  $m_\chi$ , incoming velocity  $\mathbf{v}$ , and outgoing momentum  $\mathbf{p}'_\chi$ , momentum conservation requires

$$\mathbf{q} \equiv m_\chi \mathbf{v} - \mathbf{p}'_\chi \simeq Z m_e \mathbf{v} C. \quad (9)$$

Note that the recoil energy of the ionized electron are are always negligible compared with the momentum transfer. The energy conservation requires the ionized electron get

$$\Delta E_e = \frac{1}{2}m_\chi v^2 - \frac{|m_\chi \mathbf{v} - \mathbf{q}|^2}{2m_\chi} - \frac{\mathbf{q}^2}{2Zm_e} = \mathbf{q} \cdot \mathbf{v} - \frac{\mathbf{q}^2}{2\mu_{\chi C}}, \quad (10)$$

where

$$\mu_{\chi C} = \frac{Zm_e m_\chi}{Zm_e + m_\chi} \quad (11)$$

is the DM-Cloud reduced mass and  $\Delta E_e \equiv E_{e,f} - E_{e,i}$  is the energy transferred to the ionized electron. The kinematics of the Migdal effect, single electron and REC scattering are identical, however, the dynamics differ from each other which depend on the interacting objects, in other words, on where the momentum transfer to, the nucleus, electron or the cloud.

The interaction term in the perturbation Hamiltonian of the collision between the dark matter and electron cloud with  $Ze$  is

$$H_{\text{int, C}} = - \int \frac{d^3\mathbf{q}}{(2\pi)^3} e^{i\mathbf{q} \cdot (-\mathbf{x}_\chi + \mathbf{x}_c)} \frac{\mathcal{M}_{\chi C}(q)}{4m_\chi Zm_e}, \quad (12)$$

where  $\mathbf{x}_c$  is the charge distribution position of the electron cloud and  $\mathcal{M}_{\chi C}$  is the Lorentz-invariant matrix element for dark matter scattering off electron clouds through 4-momentum transfer  $q \approx (0, \mathbf{q})$ . As the total charge of the electron cloud is  $Z$ , it is very obvious that the  $\mathcal{M}_{\chi C}$  can be reduced a similar interaction as the recoil of a single electron

$$|\mathcal{M}_{\chi C}|^2 = Z^2 |F_C(q)|^2 |\mathcal{M}_{\chi e}|^2, \quad (13)$$

in which  $F_C(q)$  is the normalized form factor talked in above section. Thus the same reduced cross section  $\bar{\sigma}_e$  can be defined to evaluate both recoils of the single electron and the cloud. In fact this is the usual way to do the comparison between detection strategies and the target, i.e.  $\sigma_p^{\text{SI}}$  spin-independent cross section for different target nuclei.

After the cloud are suddenly boosted to specific velocity  $v_C$ , it will be dragged by the static nucleus and throw away an ionized electron. As talked in above section, it is in fact a similar Migdal effect but in different Galilean frame. Thus the Rate of dragging back can be written in similar formula

$$R_C \propto |\langle \Psi_f | \Psi_{\mathbf{v}_C} \rangle|^2 \sim |\langle \psi_f | e^{i\mathbf{q}_e \cdot \mathbf{x}} | \psi_i \rangle|^2 \quad (14)$$

where  $\Psi_{\mathbf{v}_C}$  and  $\Psi_f$  are the initial and final states of the wave function of an electron cloud, and are the the single-electron states wave functions. However, be different with the Migdal effect,  $\Psi_{\mathbf{v}_C}$  is the cloud with a velocity  $\mathbf{v}_C$ , and the  $\Psi_f$  is the final state of the almost static atom.

$$\mathbf{q}_e = m_e \mathbf{v}_C = \frac{\mathbf{q}}{Z}. \quad (15)$$

The reason of this estimation is that a compact ball for the electron cloud are adopted in the whole picture, all the electrons in the cloud will move at the same velocity. Note that, though a similar  $q_e$  are use in both Migdal effect and REC, the  $q_e$  in Migdal effect is

$$\mathbf{q}_e \simeq \frac{m_e}{m_N} \mathbf{q}, \quad (16)$$

which is much smaller than  $q_e$  in Eq. (15), and this will make the phenomenology much different between the two which will be discussed in the next section.

Compared with the recoil of a single electron, the Hamiltonian is

$$H_{\text{int, e}} = - \int \frac{d^3\mathbf{q}}{(2\pi)^3} e^{i\mathbf{q} \cdot (-\mathbf{x}_\chi + \sum_{i=1}^Z \mathbf{x}_i)} \frac{\mathcal{M}_{\chi e}(q)}{4m_\chi m_e}, \quad (17)$$

and the rate

$$R_e \propto |\langle \Psi_f | H_{\text{int}} | \Psi_i \rangle|^2 \sim |\langle \psi_f | e^{i\mathbf{q} \cdot \mathbf{x}} | \psi_i \rangle|^2. \quad (18)$$

Here the initial and final state electron cloud wavefunctions  $\Psi_i$  and  $\Psi_f$  factorize only a single electron with position operator  $\mathbf{x}$  to take part in a transition between the single-electron states  $\psi_i$  and  $\psi_f$ .

The calculation of the ionization rate in REC is similar to Migdal effect and recoil of single electron, we need to integrate over the momentum transfer  $\mathbf{q}$  and the DM velocity  $\mathbf{v}$ , and sum over the final electronic states  $\Psi_f$  weighted by a delta function enforcing energy conservation. The total rate between the initial state and the final rate is

$$R_{i \rightarrow f} = \frac{\rho_\chi}{m_\chi} \int d^3v f(v) \sigma_{v_{i \rightarrow f}}, \quad (19)$$

where  $\rho_\chi$  is the local DM density, and  $f(v)$  is the Boltzmann-Maxwell distribution of the DM velocity that using the spherically symmetric approximation. For the sum over final states, the similar normalization

$$\sum_f = \frac{1}{2} \sum_{l', m'} \int \frac{k_e^3 d \ln E_e}{(2\pi)^3}, \quad (20)$$

are adopted. It is appropriate for scattering states in a spherically symmetric potential which have asymptotic momentum  $k_e = \sqrt{2m_e E_e}$  and angular momentum quantum numbers  $l'$  and  $m'$ . Here,  $E_e$  is the recoil energy of the ionized electron asymptotically far away from the ionized atom. From now on, our final state  $f$  will always be a scattered electron of energy  $E_e$ , and the initial state  $i$  will be a moving bound state of (negative) energy  $E_{nl}$  indexed by principal quantum number  $n$  and angular momentum quantum number  $l$ .

As talked above, the reduced cross section  $\bar{\sigma}_e$  is adopted of the calculation of the scattering rate. In fact, the cross section is proposed under the impulse approximation which is related to the free-particle scattering matrix element as the electron recoil spectrum per unit detector mass. The scattering of the dark matter with a single electron can treat the target electron as single-particle states of an isolated atom, described by numerical RHF bound wave functions. The velocity-averaged differential ionization cross section for electrons in the  $(n, l)$  shell.

$$\frac{d \langle \sigma_{\text{ion}}^{nl} v \rangle}{d \ln E_e} = \frac{\bar{\sigma}_e}{8\mu_{\chi e}^2} \times \int q dq |f_{\text{ion}}^{nl}(k_e, q)|^2 |F_{DM}(q)|^2 \eta(v_{min}). \quad (21)$$

where  $\eta(v_{min}) = \langle \frac{1}{v} \theta(v - v_{min}) \rangle$  is the inverse mean speed for a given velocity distribution as a function of the minimum velocity.  $v_{min}$  is the minimum velocity required for scattering. We assume a standard Maxwell-Boltzmann velocity distribution with circular velocity  $v_0 = 220\text{km/s}$  and a hard cutoff  $v_{\text{esc}} = 544\text{km/s}$ .  $\bar{\sigma}_e$  is the DM-free electron scattering cross section at fixed momentum transfer  $q_0 = \alpha m_e$ , while the  $q$ -dependence of the matrix element is encoded in the DM form-factor  $F_{DM}(q)$ . The differential ionization rate is written as

$$\frac{dR_{\text{ion}}}{d \ln E_e} = N_T \frac{\rho_\chi}{m_\chi} \sum_{nl} \frac{d \langle \sigma_{\text{ion}}^{nl} v \rangle}{d \ln E_e}, \quad (22)$$

where  $N_T$  is the number of target atoms and  $\rho_\chi = 0.4\text{GeV}/\text{cm}^3$  is the local DM density. Here, we have solved the delta function for energy conservation

$$\delta(E_e - E_{nl} + \frac{\mathbf{q}^2}{2\mu_{\chi C}} - \mathbf{q} \cdot \mathbf{v}) \quad (23)$$

to perform the integral over the DM velocity distribution, determining the  $\eta(v_{min})$ , the mean inverse DM speed in the lab frame, as a function of

$$v_{min} = \frac{|E_{nl}| + E_e}{|\mathbf{q}|} + \frac{|\mathbf{q}|}{2\mu_{\chi C}}. \quad (24)$$

The key differences between the REC and the other two processes entirely hide in the ionization form factors, which are independent of all DM properties and depends only on the electronic and nuclear structure of the target. For coherence electron clouds scattering, the analogous ionization form factor is

$$|f_{\text{ion}, C}(E_e, q)|^2 = \frac{k_e^3}{4\pi^3} Z^2 |F_C(q)|^2 \times 2 \sum_{n, l, l', m'} \left| \langle \psi_{E_e}^f | e^{i\mathbf{q}_e \cdot \mathbf{x}} | \psi_{E_{nl}}^i \rangle \right|^2. \quad (25)$$

The other two ionization form factor can be found in Ref. [19]. First there is an additional  $Z^2$  factor compared with the factor of the recoil of a single electron. This is similar to the coherent enhancement in spin-independent scattering of the nucleus. Another point is that  $q_e$  in REC will be much larger than the  $q_e$  in Migdal effect.



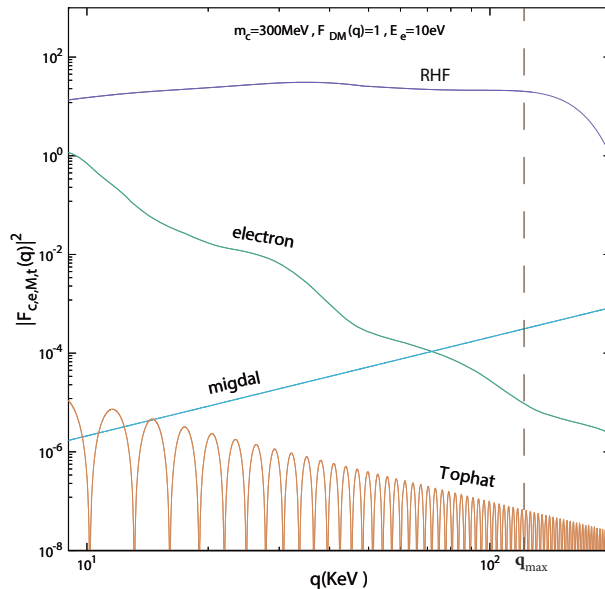


FIG. 6: Comparison with  $|f_{\text{ion}, e}|^2$  (green),  $|f_{\text{ion}, M}|^2$  (sky blue) and  $|f_{\text{ion}, C}|^2$ . For the ionization factor of the electron cloud of the Xenon atom, the purple line shows the results of RHF form factor and the brown line shows the results of the tophat. The maximum  $q$  for the REC is shown in dash line.

The numerical calculation of the ionization factor for the Xenon atom can be found in Ref. [19]. Here we chose  $m_\chi = 300\text{MeV}$ ,  $E_e = 10\text{eV}$  and  $F_{\text{DM}} = 1$  and show the difference between the three processes in the Fig. 6. In order to show the importance of the RHF electron cloud form factor, the results of the tophat shape are also shown in the figure. The interval of  $q$  is just the shaded region in the right panel of the Fig. 5. From Fig. 6, we can see that, the RHF form factor gives a much larger ionization form factor than the Migdal effect and the recoil of a single electron. However the ionization factor of the tophat shape is much smaller than the other two factors. That is reason why REC are always neglected in the literature. However, REC could dominate the ionization if we take the RHF form factor seriously. Another three points should be addressed

1. As shown in the Fig. 6,  $|f_{\text{ion}, e}|^2$  decreases quickly with the  $q$ , thus the rate of recoil of a single electron is dominated by small  $q$  region.
2.  $|f_{\text{ion}, M}|^2$  increases with the growing of  $q$ , thus the rate is dominated by large  $q$  region. Nevertheless, as the  $m_\chi$  we considered is much lighter than the mass of the nucleus, the reduced mass of the collision mainly proportional to  $m_\chi$ . Since  $q_e$  in this effect are much smaller than  $q$ , the ionization factor does not feel any suppression factor in the region of the integration.
3. The above two items are already addressed in Ref. [19], the RHF  $|f_{\text{ion}, C}|^2$  is larger than the other two ionization factors. However, the upper limit of  $q$  is

$$q_{\text{max}} = 2\mu_{\chi C}v_{\text{max}} \simeq 129.63\text{KeV}, \quad (26)$$

for a dark matter much heavier than the mass of the Xenon cloud. Note that  $v_{\text{max}}$  is taken as usual 770km/s in above equation.

With these ionization form factors, we can calculate the scattering rate and get the limits on the scattering cross section which will be discussed in the next section.

#### IV. NUMERICAL LIMITS FROM THE EXPERIMENTAL DETECTION

Following the procedure in Ref. [3], we numerically calculate the limits on the spin-independent scattering cross section from the experimental XENON100 data [35, 36] (30 kg-years) and XENON1T data [37] (1.5 tones-years).

The recoil energy  $E_e$  can induce both of the observed electrons  $n_e$  and scintillation photons  $n_\gamma$ . The numbers of quanta  $n^{(1)}$  that are produced by the step energy  $W = 13.8$  eV which is  $n^{(1)} = \text{Floor}(E_R/W)$ . The probability of the initial electron recombining with an ion is assumed as  $f_R = 0$ . The fraction of the primary quanta observed as the electrons is taken as  $f_e = 0.83$ . The corresponding uncertainties are chosen as  $0 < f_R < 0.2$ ,  $12.4 < W < 16$  eV, and  $0.62 < f_e < 0.91$ . The photons are assumed from the deexcitation of the next-to-outer shells ( $5s$ ,  $4d$ ,  $4p$ ,  $4s$ ), whose energies correspond to (13.3, 63.2, 87.9, 201.4) eV. Due to the photoionization effect, these photons can respectively create an additional quanta numbers  $n^{(2)} = (n_{5s}, n_{4d}, n_{4p}, n_{4s}) = (0, 4, 6 - 10, 3 - 15)$  as shown in the Table I [6]. The electron event  $n_e$  can be obtained by binomial distribution. The ionized electrons will convert into the photoelectron (PE). The PE number is produced by an event of  $n_e$  which obey Gaussian distribution with mean  $n_e\mu$  and width  $\sqrt{n_e\sigma}$ , where  $\mu = 19.7(11.4)$  and  $\sigma = 6.2(2.8)$  for XENON100 (XENON1T). Note that the data in the range of [165, 275] of the XENON1T data are adopted for our numerical evaluation.

shell	$5p^6$	$5s^2$	$4d^{10}$	$4p^6$	$4s^2$
Binding Energy[eV]	12.6	25.7	75.6	163.5	213.8
Additional Quanta	0	0	4	6-10	3-15

TABLE I: Additional quanta of the ionization of Xenon.

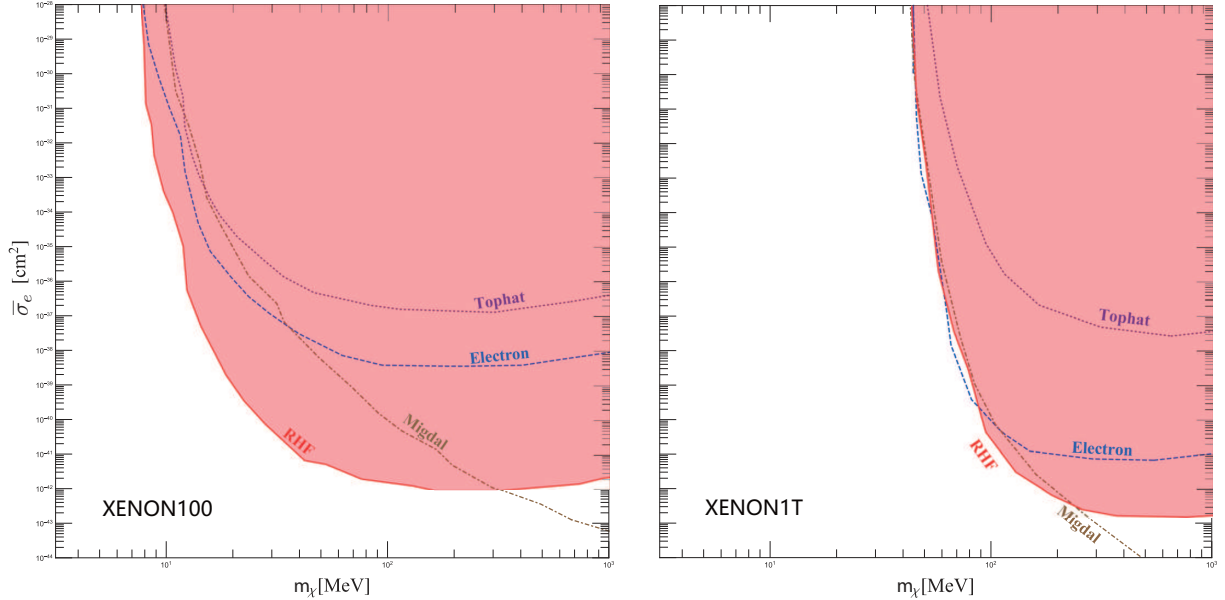


FIG. 7: The limits of the cross sections and dark matter mass from Xenon100 (left panel) and Xenon1T(right panel). The dash (dot dash) lines show limits on the recoil of single electron and the Migdal effect. The dot line show the result of tophat model of the electron cloud, and the shaded regions show results of RHF form factor.

Fig. 7 shows the numerical results of the limits from Xenon100 (left panel) and Xenon1T (right panel) data. The results of limits on the recoil of a single electron and Migdal effect are also shown for the comparison. We can see that, in the range of  $m_\chi \gtrsim 100\text{MeV}$ , the limits of the RHF form factor are much stringent than the recoil of a single electron, almost 4 orders stronger. This can be easily understood that the coherent enhancement of  $Z^2(54^2)$  factor and a sufficiently large RHF  $F(q)$  in the interval of the rate integral Eq. (21). Of course, the limits on the tophat model of the electron cloud are negligible. Note that, since recoil of a single electron and recoil of the electron cloud originate from the same fundamental interaction, thus in principle both recoils should be added together and the summation gives a more comprehensive limits on the cross section. The constraints of the Xenon1T data released below the 100MeV, however, the Xenon100 data can maintain the constraints to about 10MeV. The reason for this can be shown in Fig. 8 which shows the observed events versus photonelectrons (PE) from the Xenon100 and Xenon1T experimental data for  $m_\chi = 100\text{MeV}$ . The left panel shows the  $\bar{\sigma}_e = 1 \times 10^{-39}\text{cm}^{-2}$  result for Xenon100, and the right panel shows the  $\bar{\sigma}_e = 1 \times 10^{-40}\text{cm}^{-2}$  results for Xenon1T. One can check that, the lighter dark matter ( $< 100\text{MeV}$ ) in the recoil of a single electron and REC mainly cause different distribution in small PE number regions. In the numerical calculation we chose 80-190 PE bins of the Xenon100 for the constraints, while we chose 165-275 PE bins

of the Xenon1T for the constraints. Thus the Xenon100 give a better performance when the dark matter mass lighter than 100 MeV.

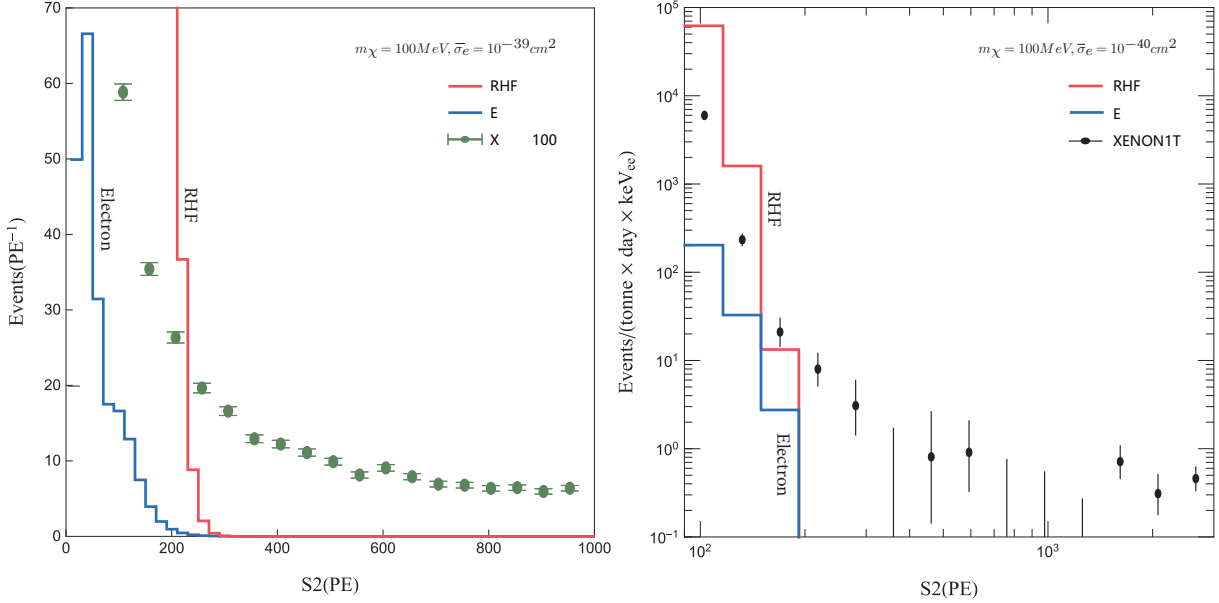


FIG. 8: Observed events versus photonelectrons (PE) from Xenon100 (left panel) and Xenon1T (right panel) data for  $m_\chi = 100\text{MeV}$  and for Xenon100  $\bar{\sigma}_e = 1 \times 10^{-39}\text{cm}^{-2}$  while for Xenon1T,  $\bar{\sigma}_e = 1 \times 10^{-40}\text{cm}^{-2}$ .

As for the comparison with Migdal effect, the limits on the RHF form factor are more stringent than the Migdal effect below about 400MeV (200MeV) from Xenon100 (Xenon1T) data. The reason has been addressed above that the upper limit of the rate integral Eq. (21)  $q_{\text{max}}$  in the Migdal effect can extend to a much larger value when dark matter mass is much lighter than the target nucleus. The ionization form factor can grow up to a sufficiently large value. Thus, the Migdal effect give a better performance in heavy dark matter region.

## V. CONCLUSION

The searching for sub-GeV dark matter is a hot topic at the cutting edge of physics research. However, as the sensitivity lost for the light dark matter detection, the traditional strategies for detecting WIMP-type dark matter are no longer feasible. A novel detection are proposed that the electron cloud are boosted by the dark matter and throw away an electron when it is dragged back by the heavy nucleus, namely the coherent scattering of the electron cloud of the atom. The processes can be considered as an similar Migdal effect but in different Galilean fame. At first glance, the form factor  $F(q)$  will decrease quickly with the inverse of the radius of the atom, as shown in the tophat, dipole and Gaussian model shape. Thus this effect is generally negligible compared with the recoil of a single electron and the Migdal effect. However, the survey in the X-ray diffraction show that the atomic form factor are much complicate than the naive consideration. The results of the relativistic Hartree-Fock method gives non-trivial shapes of of the atom. We show that the corresponding form factors do not conflict with charge distribution in the coordinate space. We also show that the collision between the sub-GeV dark matter and the electron cloud is similar to the X-ray diffraction. At least, The RHF form factor can be proposed to be tried in the estimation of the scattering rate.

Having equipped with the RHF form factor and impulse approximation, we proceed to show the detailed calculation of recoil of the electron cloud. The kinetics, the fiducial cross section and the corresponding calculation of detection rate are given analytically. After that, we show the constraints on the cross section from the current experimental measurements. The Xenon100 and Xenon1T data are adopted for the constraints. The comparison between the other two processes are also discussed. We found that the limits of the RHF form factor are much stringent than the recoil of a single electron, almost 4 orders stronger. The constraints of the Xenon1T data released below the 100MeV, however, the Xenon100 data can maintain the constraints to about 10MeV. The limits on the RHF form factor are more stringent than the Migdal effect below about 400MeV (200MeV) from Xenon100 (Xenon1T) data, due to the extended interval of the rate integration. Another thing should be emphasized is that, the recoil of a single electron

and recoil of the electron cloud originate from the same basic interaction, thus in principle both recoils should be added together and the summation gives a more comprehensive limits on the cross section.

The process we proposed and the corresponding results seem promising and novel. However, the key point of our work is that whether the RHF form factor can be used in the detection of the dark matter, which we only have neutral attitude on it.

## VI. ACKNOWLEDGEMENTS

We thank Nick Houston, Lei Wu and Bin Zhu for their helpful discussions. This work was supported by the Natural Science Foundation of China under grant number 11775012.

- 
- [1] G. Bertone, D. Hooper, and J. Silk, *Phys. Rept.* **405**, 279 (2005), arXiv:hep-ph/0404175 .
- [2] R. Essig, J. Mardon, and T. Volansky, *Phys. Rev. D* **85**, 076007 (2012), arXiv:1108.5383 [hep-ph] .
- [3] R. Essig, A. Manalaysay, J. Mardon, P. Sorensen, and T. Volansky, *Phys. Rev. Lett.* **109**, 021301 (2012), arXiv:1206.2644 [astro-ph.CO] .
- [4] R. Essig, M. Fernandez-Serra, J. Mardon, A. Soto, T. Volansky, and T.-T. Yu, *JHEP* **05**, 046 (2016), arXiv:1509.01598 [hep-ph] .
- [5] J.-W. Chen, H.-C. Chi, C. P. Liu, C.-L. Wu, and C.-P. Wu, *Phys. Rev. D* **92**, 096013 (2015), arXiv:1508.03508 [hep-ph] .
- [6] R. Essig, T. Volansky, and T.-T. Yu, *Phys. Rev. D* **96**, 043017 (2017), arXiv:1703.00910 [hep-ph] .
- [7] Q.-H. Cao, R. Ding, and Q.-F. Xiang, *Chin. Phys. C* **45**, 045002 (2021), arXiv:2006.12767 [hep-ph] .
- [8] I. M. Bloch, A. Caputo, R. Essig, D. Redigolo, M. Sholapurkar, and T. Volansky, *JHEP* **01**, 178 (2021), arXiv:2006.14521 [hep-ph] .
- [9] S. Knapen, J. Kozaczuk, and T. Lin, *Phys. Rev. D* **104**, 015031 (2021), arXiv:2101.08275 [hep-ph] .
- [10] Y. Hochberg, Y. Kahn, N. Kurinsky, B. V. Lehmann, T. C. Yu, and K. K. Berggren, *Phys. Rev. Lett.* **127**, 151802 (2021), arXiv:2101.08263 [hep-ph] .
- [11] A. Migdal, *Sov.Phys.JETP* **9**, 1163 (1939).
- [12] J. D. Vergados and H. Ejiri, *Phys. Lett. B* **606**, 313 (2005), arXiv:hep-ph/0401151 .
- [13] C. C. Moustakidis, J. D. Vergados, and H. Ejiri, *Nucl. Phys. B* **727**, 406 (2005), arXiv:hep-ph/0507123 .
- [14] H. Ejiri, C. C. Moustakidis, and J. D. Vergados, *Phys. Lett. B* **639**, 218 (2006), arXiv:hep-ph/0510042 .
- [15] R. Bernabei *et al.*, *Int. J. Mod. Phys. A* **22**, 3155 (2007), arXiv:0706.1421 [astro-ph] .
- [16] M. Ibe, W. Nakano, Y. Shoji, and K. Suzuki, *JHEP* **03**, 194 (2018), arXiv:1707.07258 [hep-ph] .
- [17] M. J. Dolan, F. Kahlhoefer, and C. McCabe, *Phys. Rev. Lett.* **121**, 101801 (2018), arXiv:1711.09906 [hep-ph] .
- [18] N. F. Bell, J. B. Dent, J. L. Newstead, S. Sabharwal, and T. J. Weiler, *Phys. Rev. D* **101**, 015012 (2020), arXiv:1905.00046 [hep-ph] .
- [19] D. Baxter, Y. Kahn, and G. Krnjaic, *Phys. Rev. D* **101**, 076014 (2020), arXiv:1908.00012 [hep-ph] .
- [20] R. Essig, J. Pradler, M. Sholapurkar, and T.-T. Yu, *Phys. Rev. Lett.* **124**, 021801 (2020), arXiv:1908.10881 [hep-ph] .
- [21] G. Grilli di Cortona, A. Messina, and S. Piacentini, *JHEP* **11**, 034 (2020), arXiv:2006.02453 [hep-ph] .
- [22] C. P. Liu, C.-P. Wu, H.-C. Chi, and J.-W. Chen, *Phys. Rev. D* **102**, 121303 (2020), arXiv:2007.10965 [hep-ph] .
- [23] S. Knapen, J. Kozaczuk, and T. Lin, *Phys. Rev. Lett.* **127**, 081805 (2021), arXiv:2011.09496 [hep-ph] .
- [24] Z.-L. Liang, C. Mo, F. Zheng, and P. Zhang, *Phys. Rev. D* **104**, 056009 (2021), arXiv:2011.13352 [hep-ph] .
- [25] V. V. Flambaum, L. Su, L. Wu, and B. Zhu, (2020), arXiv:2012.09751 [hep-ph] .
- [26] N. F. Bell, J. B. Dent, B. Dutta, S. Ghosh, J. Kumar, and J. L. Newstead, *Phys. Rev. D* **104**, 076013 (2021), arXiv:2103.05890 [hep-ph] .
- [27] J. F. Acevedo, J. Bramante, and A. Goodman, (2021), arXiv:2108.10889 [hep-ph] .
- [28] F. J., *Journal of Physics A Mathematical & General* **11(10)**, 1915 (1978).
- [29] H. M. Xiaoyong Chu, Camilo Garcia-Cely, *Phys. Rev. Lett.* **124**, 041101 (2020), arXiv:1901.00075 [hep-ph] .
- [30] B. Z. Wenyu Wang, Wu-Long Xu, (2021), arXiv:2108.07030v1 [hep-ph] .
- [31] P. A. Doyle and P. S. Turner, *Acta Cryst.* **A24**, 390 (1968).
- [32] D. T. Cromer and J. B. Mann, *Acta Cryst.* **A24**, 321 (1968).
- [33] e. a. E, Prince, *International Tables for Crystallography* **C**, 1 (2016).
- [34] M. A. O. A. G. Fox and M. A. Tabbernor, *Acta Cryst.* **A45**, 786 (1989).
- [35] E. Aprile *et al.* (XENON100), *Astropart. Phys.* **35**, 573 (2012), arXiv:1107.2155 [astro-ph.IM] .
- [36] E. Aprile *et al.* (XENON), *Phys. Rev. D* **94**, 092001 (2016), [Erratum: *Phys.Rev.D* 95, 059901 (2017)], arXiv:1605.06262 [astro-ph.CO] .
- [37] E. Aprile *et al.* (XENON), *Phys. Rev. Lett.* **123**, 251801 (2019), arXiv:1907.11485 [hep-ex] .